# Debonding of Stitched Composite Joints: Testing and Analysis

E.H. Glaessgen†, I.S. Raju and C.C. Poe, Jr.
NASA Langley Research Center, Hampton, VA 23681-0001, U.S.A.

## Abstract

The effect of stitches on the failure of a single lap joint configuration was determined in a combined experimental and analytical study. The experimental study was conducted to determine debond growth under static monotonic loading. The stitches were shown to delay the initiation of the debond and provide load transfer beyond the load necessary to completely debond the stitched lap joint. The strain energy release rates at the debond front were calculated using a finite element-based technique. Models of the unstitched configuration showed significant values of modes I and II across the width of the joint and showed that mode III is zero at the centerline but increases near the free edge. Models of the stitched configuration showed that the stitches effectively reduced mode I to zero, but had less of an effect on modes II and III.

## Introduction

Stitched warp-knit textile composite materials are currently being considered for use in primary aerospace structures. Structures manufactured from these materials offer advantages in manufacturability and damage tolerance over conventional composite and metallic structures. However, it is often impossible to manufacture a complete component as an integral unit, and hence separate sections of the component need to be joined together. Rather than bolting or bonding sections, stitching is used in the textile composites discussed here.

The objective of this paper is to quantify the effect of Kevlar stitches on the response of lap joints in warp-knit carbon epoxy textile composites under monotonic tensile loading. Failure mechanisms and failure loads of unstitched and stitched lap joints will be determined using a combined analytical and experimental technique. Comparisons will be made between the experimentally determined failure loads of the stitched and similar unstitched lap joint panels to assess the effectiveness of the stitches in preventing delamination growth.[1]

## Lap Joint Configuration

A stitched lap joint subjected to remote tensile loading is shown in Figure 1. The major configurational parameters of this joint are the length of the composite, $L_1$, the length of the overlap, $L_2$, the width of the coupon, $b$, the thickness of the coupon, $t$, and the debond length, $a$. The equivalent laminate stacking sequence of the material is $(45/-45/0/90/0/-45/45)_{2s}$ for both of the joined laminates.

Specimens were machined from the unstitched and stitched portion of the panel to the dimensions given in Table 1. The specimens were loaded in monotonic tension at a rate of 0.127 cm./min. to initiate and grow debonds at the ends of the lap joints. The failure loads for coupons with and without stitching were determined. The increase in debond length with increasing load was determined using a radiographic technique.

## Finite Element Analysis

The method of analysis involves the use of plate elements to model the configuration, nonlinear fastener elements to model the stitches and multipoint constraints to model the contact problem. The stitches are modeled as nonlinear fastener elements with axial and shear compliances determined using independent flatwise tension and double lap shear tests. Only the fastener elements behind the debond front carry load since the upper and lower plate elements ahead of the debond front are coupled using constraint equations to have identical translational displacements. The stitch location spacing presented in Table 1 coincides with plate element nodal locations. This modeling technique allows an experimentally determined load vs. deflection behavior to be considered for each stitch. The behavior includes the local effects of the stitch debonding from the laminate in addition to nonlinearity of the stitch material itself. Failure of the stitches occurs at a load of 258 N per stitch in tension and 169 N per stitch in shear.[2]

In these analyses, the laminates are assumed to be homogeneous with axial properties determined experimentally and all others estimated using the equivalent stacking sequence and classical lamination theory as

$$E_{11}=80.7\ GPa \quad \mu_{12}=17.2\ GPa \quad \upsilon_{12}=0.40$$
$$E_{22}=35.4\ GPa \quad \mu_{13}=12.2\ Gpa \quad \upsilon_{13}=0.30$$
$$E_{33}=12.3\ GPa \quad \mu_{23}=6.07\ Gpa \quad \upsilon_{23}=0.30$$

where $E_{ii}$, $\mu_{ij}$, $\upsilon_{ij}$ (i,j=1,2,3) are the Young's moduli, shear moduli, and Poisson's ratio, respectively, and the subscripts 1,2,3 represent the fiber, transverse and out-of-plane directions, respectively.

## Experimental Results

Since a limited amount of the material was available, only two replicates of each specimen configuration were tested. The failure loads of these specimens are presented in Table 2.

Figures 2(a) and 2(b) present the damage near failure within representative lap joints of the unstitched and stitched configurations, respectively. Figure 2(a) shows the unstitched lap joint of length $L_2$=9.37 cm. with a delamination of length, $a$, growing from the top of the lap ($x=+L_2$ in Figure 1) at a load of 19.1 kN. No debonds were observed growing near the bottom of the lap ($x=0$ in Figure 1). This could be the result of a small asymmetry in the specimen or load frame and is likely due to the debond at the top of the lap initiating first and relieving the driving force at the bottom of the lap.

The primary debond shown in Figure 2(a) grew at the interface of 45° yarns. A split initiated in the 45° yarns and allowed a secondary debond to initiate and grow between the 45° and 0°

Table 1: Test Specimen Dimensions

| Panel | Stitch Column Spacing, $S_x$, cm. | Stitch Row Spacing, $S_y$, cm. | Thickness, t, cm. | Width, b, cm. | Lap length, $L_2$, cm. | Length, $L_1$, cm. |
|---|---|---|---|---|---|---|
| 1 | 0.318 | 0.318 | 0.279 | 2.54 | 9.37 | 68.6 |

† Resident Research Associate, National Research Council

yarns as shown in Figure 2(a). Catastrophic failure due to unstable debond growth was observed at 20.7 kN.

Table 2: Test Specimen Failure Loads

| Specimen | Unstitched (U) or Stitched (S) | Failure Load, kN |
|---|---|---|
| Slap 1-1 | U | 20.7 |
| Slap 1-2 | U | 19.6 |
| Slap 1-1S | S | 52.6 |
| Slap 1-2S | S | 51.7 |

Figure 2(b) shows a completely debonded lap joint that maintained a load of 49.1 kN. Debonds initiated and grew from both ends of the joint completely debonding the lap joint. Final failure occurred at 52.6 kN and was not due to stitch failure but was due to a tensile and bending stress failure at the ends of the lap. The value of 52.6 kN may then be treated as a lower bound of load carrying capability for this specimen. The average failure load of the stitched lap joints was 2.6 times the failure load of the unstitched lap joints.

## Analytical Results

Since the single lap joint configuration has a finite width, all three modes of strain energy release rate operate on the debond. Also, although a straight debond front is employed to simplify the analyses, a variation in both strain energy release rate, $G$, and stitch force may exist along the length ($x$-) and across the width ($y$-) of the lap joint. Thus, G-values are determined at a location near the centerline (A) and at a location near the free edge (B). Locations $A$ and $B$ correspond to stitch row 1 and stitch row 4 in Figure 1 and are located at $y$=0.159 cm. and $y$=1.11 cm., respectively, from the configuration centerline.

For convenience and clarity, the individual modes of energy release rate are plotted as functions of debond length. Because of symmetries and antisymmetries of the lap joint configuration, the curves presented in Figure 3 are valid for the complete lap joint.

The values of strain energy release rate for loads corresponding to the debond lengths in Figure 3 are significantly greater than the $G_{Ic}$ and $G_{IIc}$ values determined for the 3501-6 resin used in the specimens.[3] Both the unstitched and stitched lap joint configurations are able to sustain these high $G$-values due to several energy absorbing phenomena. In the unstitched material, splitting of the 45° yarns and the formation and growth of a secondary debond between the 45° and 0° yarns seen in Figure 2(a) contribute to the apparent high value of fracture toughness. In the stitched material, there is also some damage within the stacks of material as shown in Figure 2(b). This occurs over only a small portion of the debonded length of the stitched lap joint. The plate element-based analyses can predict the effective values of $G$ as seen in Figure 3 that can then be used as ranking parameters.

Figure 3(a) shows $G$-values plotted against debond length for the unstitched configuration with a debond at only one end of the single lap joint. The figure shows two nonzero components of $G$ at location $A$ and three nonzero components of $G$ at location $B$ for the unstitched configuration. Mode I becomes increasingly significant at both locations as the debond length increases. Mode II is the largest component of energy release rate and also increases with increasing debond length. Mode III has a value near zero (thus, not shown) at location $A$ but increases near the edge.

Figure 3(b) shows the $G$-values plotted as functions of debond length for the stitched configuration with a debond at each end of the single lap joint. The figure shows one nonzero component of $G$ at location $A$ and two nonzero components of $G$ at location $B$ for the stitched configuration. For all debond lengths at both locations, the mode I component is near zero. As with the unstitched configuration, mode II is the dominant component and is seen to increase with debond length. Although $G_{II}$ increases with increasing debond length, the stitches keep the debond growth stable. Mode II is larger near the configuration centerline for short debonds but is larger near the configuration edge for longer debonds. As in the unstitched configuration, Mode III has a value near zero at location A but increases near the edge.

## Concluding Remarks

The effect of stitches on the failure of single lap joint configuration was studied. An experimental study was conducted to determine the loads necessary to grow the debond through complete debonding of the specimens. An analytical investigation was performed using finite element analyses and the virtual crack closure technique to compute strain energy release rates and stitch forces.

Radiographs of the unstitched lap joint indicated that a debond initiated and grew from only one end of the lap joint. Radiographs of the stitched lap joint indicated that the debond grew from both ends of the lap joint with neither debond dominating the other. For the configurations considered, the failure load of the stitched lap joints was about two and a half times the failure load of the unstitched lap joints.

Models of the unstitched configuration showed that the nonzero components of strain energy release rate vary nearly linearly with debond length. All three modes increase with increasing debond length at both near the configuration centerline and near the configuration free edge. Mode II is the largest of the three components, while mode III is the smallest.

Models of the stitched configuration showed that only one nonzero component of $G$ exists near the centerline while two nonzero components exist near the free edge. The stitches reduce $G_I$ to near zero values for all debond lengths. However, the stitches are much less effective in reducing $G_{II}$ as it is the dominant component and is seen to increase over the entire range of debond lengths considered. Mode II becomes larger near the free edge than near the centerline with increasing load. Mode III is significant only near the free edge.

## References


[1.] Glaessgen, E.H., Raju, I.S. and Poe, C.C., "Delamination and Stitch Failure in Stitched Composite Joints," *40th AIAA/ASME/ASCE/AHS Structures, Structural Dynamics and Materials Conference*, AIAA Paper 99-1247, 1999.

[2.] Adams, D.O., "Stitch Compliance in Delaminated Composites," *29th SAMPE Technical Conference*, Orlando, FL, October 28-31, 1997.

[3.] Reeder, J.R., "A Bilinear Failure Criterion for Mixed-Mode Delamination," *ASTM STP 1206*, E.T. Camponeschi, Jr., Ed., ASTM, Philadelphia, PA, 1993, pp. 303-322.

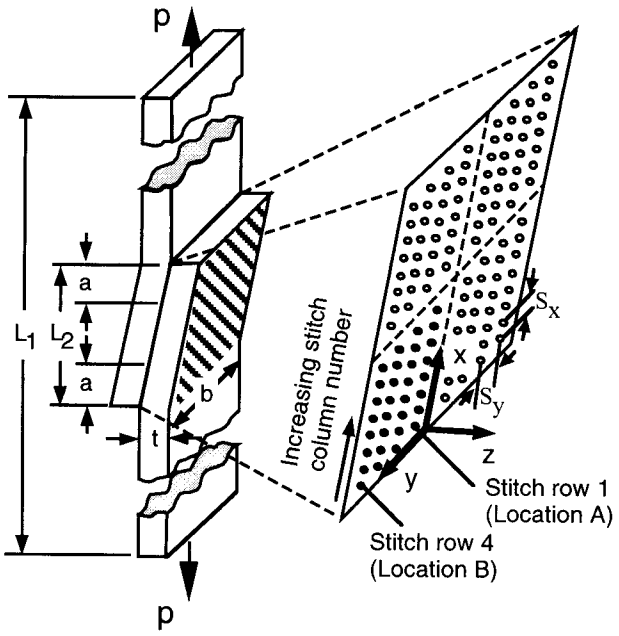


Figure 1. Stitched joint configurations.

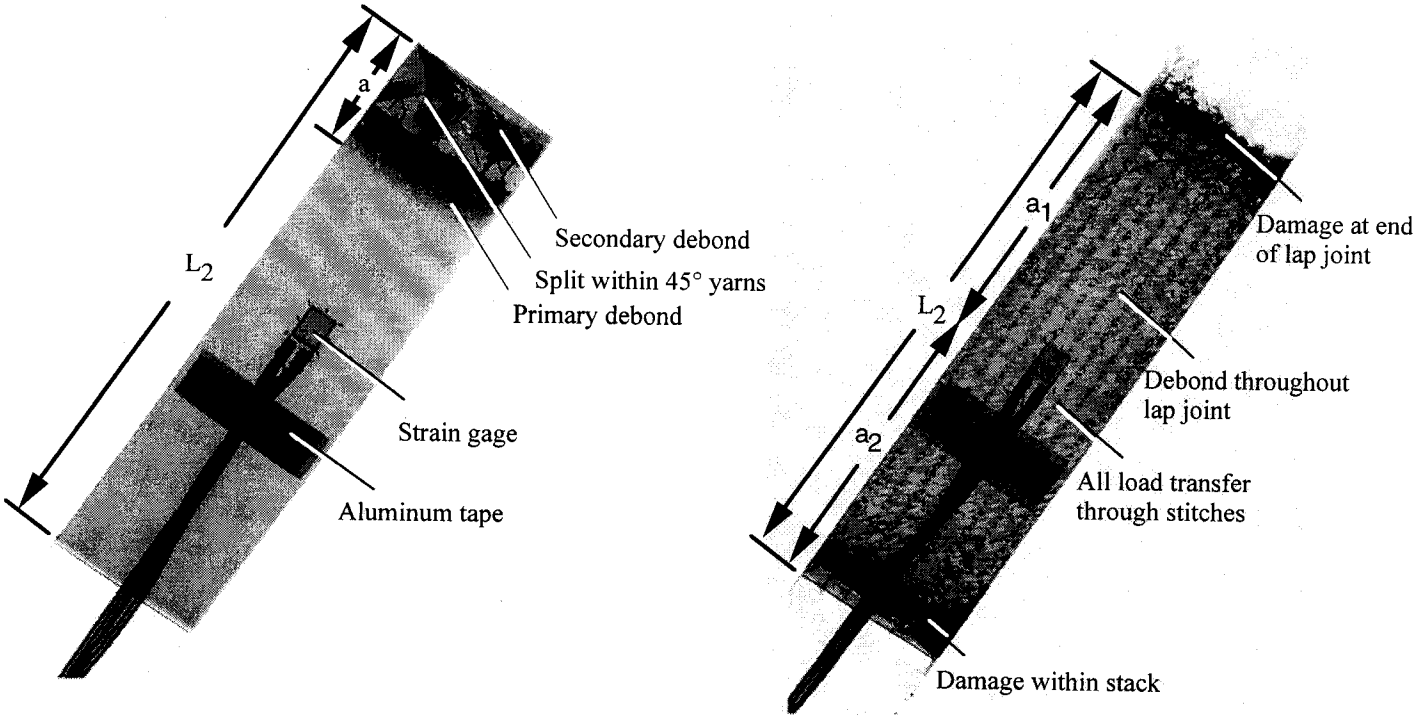


(a) Unstitched specimen at P=19.1 kN (a=1.98 cm.)

(b) Stitched specimen at P=49.1 kN ($a_1$=4.68 cm., $a_2$=4.68 cm.)

Figure 2. Radiographs showing debond in lap joint.

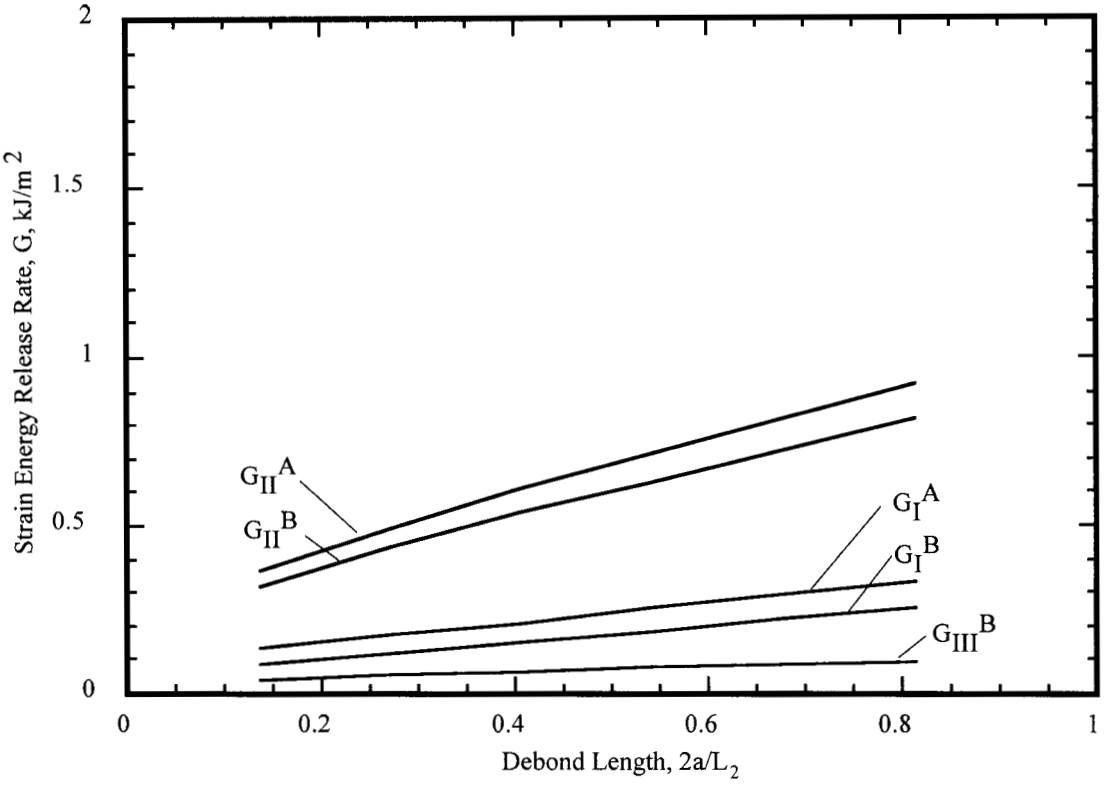


(a) Strain energy release rate in unstitched lap joint

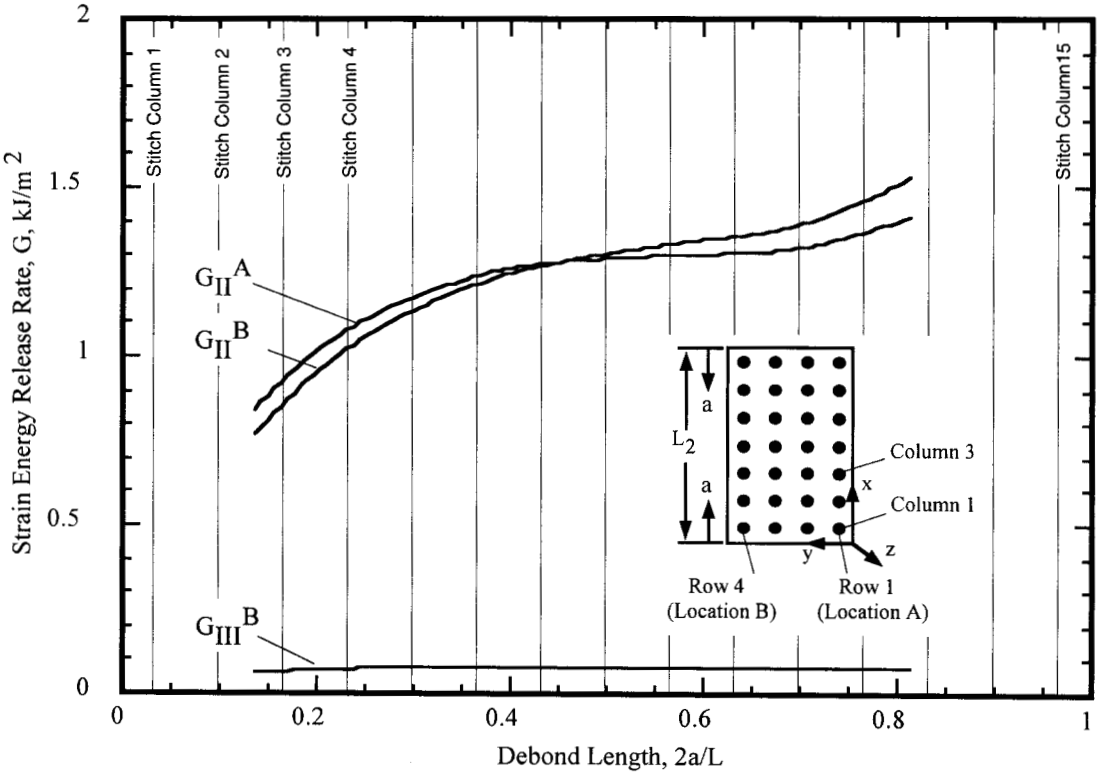


(b) Strain energy release rate in stitched lap joint

Figure 3. Strain energy release rates.